R. E., & Williams, R. J. P., Eds.) p 95, Academic Press, New York.
Snyder, G. H., Rowan, R., Karplus, S., & Sykes, B. D. (1975) *Biochemistry 14*, 3765.
Stone, D., Phillips, A. W., & Burchall, J. J. (1977) *Eur. J. Biochem. 72*, 613.
Wagner, G., De Marco, A., & Wüthrich, K. (1975) *J. Magn. Reson. 20*, 565.

Mechanism of Actomyosin Adenosine Triphosphatase. Evidence That Adenosine 5′-Triphosphate Hydrolysis Can Occur without Dissociation of the Actomyosin Complex†

Leonard A. Stein,‡ Richard P. Schwarz, Jr., P. Boon Chock, and Evan Eisenberg*

ABSTRACT: We have investigated the steps in the actomyosin ATPase cycle that determine the maximum ATPase rate (V_{max}) and the binding between myosin subfragment one (S-1) and actin which occurs when the ATPase activity is close to V_{max}. We find that the forward rate constant of the initial ATP hydrolysis (initial P_i burst) is about 5 times faster than the maximum turnover rate of the actin S-1 ATPase. Thus, another step in the cycle must be considerably slower than the forward rate of the initial P_i burst. If this slower step occurs only when S-1 is complexed with actin, as originally predicted by the Lymn–Taylor model, the ATPase activity and the fraction of S-1 bound to actin in the steady state should increase almost in parallel as the actin concentration is increased. As measured by turbidity determined in the stopped-flow apparatus, the fraction of S-1 bound to actin, like the ATPase activity, shows a hyperbolic dependence on actin concentration, approaching 100% asymptotically. However, the actin concentration required so that 50% of the S-1 is bound to actin is about 4 times greater than the actin concentration required for half-maximal ATPase activity. Thus, as previously found at 0 °C, at 15 °C much of the S-1 is dissociated from actin when the ATPase is close to V_{max}, showing that a slow first-order transition which follows the initial P_i burst (the transition from the refractory to the nonrefractory state) must be the slowest step in the ATPase cycle. Stopped-flow studies also reveal that the steady-state turbidity level is reached almost instantaneously after the S-1, actin, and ATP are mixed, regardless of the order of mixing. Thus, the binding between S-1 and actin which is observed in the steady state is due to a rapid equilibrium between S-1–ATP and acto–S-1–ATP which is shifted toward acto–S-1–ATP at high actin concentration. Furthermore, both S-1–ATP and S-1–ADP·P_i (the state occurring immediately after the initial P_i burst) appear to have the same binding constant to actin. Thus, at high actin concentration both S-1–ATP and S-1–ADP·P_i are in rapid equilibrium with their respective actin complexes. Although at very high actin concentration almost complete binding of S-1–ATP and S-1–ADP·P_i to actin occurs, there is no inhibition of the ATPase activity at high actin concentration. This strongly suggests that both the initial P_i burst and the slow rate-limiting transition which follows (the transition from the refractory to the nonrefractory state) occur at about the same rates whether the S-1 is bound to or dissociated from actin. We, therefore, conclude that S-1 does not have to dissociate from actin each time an ATP molecule is hydrolyzed.

It is now generally accepted that muscle contraction is caused by interdigitating myosin and actin filaments sliding past each other. This sliding process appears to be driven by a cyclic interaction of myosin cross bridges with actin and ATP (Huxley, 1969; Huxley, 1974). For an understanding of this cyclic interaction in vivo, considerable effort has been devoted to studying the kinetics of the actomyosin ATPase in vitro. The major goal of these studies, most of which have employed the soluble fragments of myosin, heavy meromyosin (HMM), and subfragment 1 (S-1), has been to determine the simplest kinetic model which is consistent with both pre-steady-state and steady-state kinetic data.

In 1971, on the basis of their pre-steady-state kinetic studies, Lymn & Taylor (1971) proposed the model shown in Scheme I for the actomyosin ATPase. In this model the number of asterisks on the myosin intermediates qualitatively represents the amount of fluorescence shown by these intermediates (Bagshaw et al., 1974). This model was based on data obtained at 20 °C which showed that, at relatively low actin concentration, complete dissociation of the acto–HMM complex by ATP occurs before hydrolysis of the ATP in the initial P_i burst ($M^*{\cdot}T \rightarrow M^{**}{\cdot}D{\cdot}P_i$). Sleep & Taylor (1976), working at low temperature, confirmed this basic finding. However, it has never been clear what rate constants are required in this model to explain the steady-state data of Eisenberg (Eisenberg & Moos (1968, 1970)). Since the initial P_i burst was found to be faster than the steady-state maximum

Scheme I

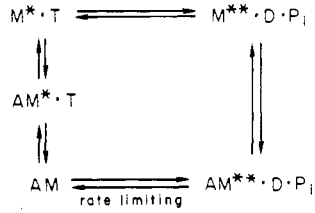

† From the Laboratory of Cell Biology and the Laboratory of Biochemistry, National Heart, Lung, and Blood Institute, National Institutes of Health, Bethesda, Maryland 20014. *Received February 8, 1979.* A preliminary communication of this work has been presented at the Biophysical Society Meeting (Stein et al., 1979).
‡ This work was performed during the tenure of the George Meany Postdoctoral Fellowship awarded by the Muscular Dystrophy Association to L.A.S.

Scheme II

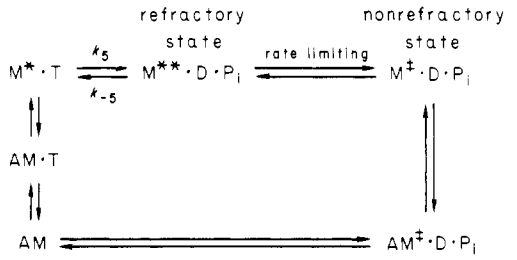

actin-activated ATPase rate (V_{max}), Lymn & Taylor (1971) suggested that the slowest step in the cycle was the release of products (AM**·D·P$_i$ → AM). However, it is then unclear how this model can account for the data of Eisenberg and his co-workers which showed that, at low temperature, when the actin-activated ATPase rate is close to V_{max}, most of the HMM or S-1 is dissociated from actin (Eisenberg & Kielley, 1972; Fraser et al., 1975). Marston (1978) and Wagner & Weeds (1979) recently confirmed this finding by using the same kinetic method as Eisenberg & Kielley (1972).

To explain their steady-state data, Eisenberg & Kielley (1972) proposed the refractory-state kinetic model shown in Scheme II. In this model, as in the Lymn–Taylor model, dissociation of the acto–S-1 complex by ATP occurs before the initial P$_i$ burst. But, following the initial P$_i$ burst rather than the S-1 rebinding directly to actin, it first undergoes the rate-limiting transition from the refractory to the nonrefractory state. Thus, this model predicts that the transition from the refractory to the nonrefractory state will limit the rate of rebinding of S-1 to actin. The pre-steady-state kinetic data of Chock et al. (1976) showed that, at high actin concentration during a single cycle of ATP hydrolysis, the rate of rebinding of S-1 to actin did, indeed, level off at a rate equal to V_{max}. These data support the refractory-state model, assuming, first, that the initial P$_i$ burst is not the rate-limiting step in the cycle and, second, that there is complete dissociation of the acto–S-1 complex when ATP binds to the acto–S-1. This second assumption is particularly important to test since the refractory-state model, in its simplest form, predicts that, at saturating actin concentration, all of the S-1 will be dissociated from actin, yet it has always been observed that a small fraction of the S-1 or HMM binds to actin as the steady-state ATPase activity approaches V_{max} (Eisenberg & Kielley, 1972; Fraser et al., 1975). This binding could be due to a rate-limiting step in the cycle following reassociation of the S-1 and actin, as suggested in the original Lymn–Taylor model (Scheme I), or it could be due to a rapid equilibrium between M*·T and AM*·T with incomplete dissociation of the AM*·T complex.

In the present study, we first compared the rate of V_{max} with the rate of the initial P$_i$ burst, making use of the recent finding that the maximal rate of the fluorescence change induced by ATP represents the rate of the initial P$_i$ burst (Johnson & Taylor, 1978; Chock et al., 1979). We then measured the binding of S-1 to actin in the presence of ATP, using as a measure of binding absorbance determined directly in the stopped-flow apparatus.

Our results show that the initial P$_i$ burst is not the slowest step in the kinetic cycle; another rate-limiting step must follow the initial P$_i$ burst. Our results also show that binding between S-1 and actin does occur during steady-state ATP hydrolysis at high actin concentration, with the fraction of S-1 bound to actin approaching 1 asymptotically at high actin concentration. However, the level of binding observed between S-1 and actin in the steady state is achieved almost instantaneously on mixing S-1, actin, and ATP, regardless of the order of mixing. Therefore, the binding observed in the steady state is not due to AM**·D·P$_i$ accumulating in front of a rate-limiting step as proposed in the original Lymn–Taylor model. Rather, it is due to a rapid equilibrium occurring between M*·T and AM*·T, which is shifted toward AM*·T at high actin concentration. Our results also suggest that both M*·T and M**·D·P$_i$ have the same binding constant to actin and at high actin concentration are in rapid equilibrium with AM*·T and AM**·D·P$_i$, respectively. However, the presence of significant amounts of AM*·T and AM**·D·P$_i$ is not accompanied by detectable inhibition of the acto–S-1 ATPase. Furthermore, 4 times more actin is required to reach half-maximal binding of S-1 to actin than to reach half-maximal ATPase activity. Computer modelling of these data strongly suggests that both the initial P$_i$ burst and the rate-limiting transition from the refractory to the nonrefractory state occur at about the same rate whether or not the S-1 is complexed with actin. Therefore, neither the Lymn–Taylor model nor the refractory-state model as originally proposed is correct. The refractory state (M**·D·P$_i$) can bind weakly to actin, and dissociation of the acto–S-1 complex is not a mandatory step in the ATPase cycle.

Materials and Methods

Proteins. Myosin was purified from rabbit back and leg muscles according to the method of Kielley & Harrington (1960). S-1 was prepared by the method of Weeds & Taylor (1975) except that 0.5 mM DTT was included in all of our solutions. S-1 containing the alkali 1 light chain [(A-1)S-1] was also prepared by the method of Weeds & Taylor (1975). F-actin was prepared by using a modified method of Spudich & Watt (1971) (Eisenberg & Kielley, 1974). Protein concentrations were measured spectrophotometrically. The extinction coefficients used for a 1 mg/mL solution at 280 nm were 0.75 cm^{-1} for both S-1 and (A-1)S-1 and 1.15 cm^{-1} for F-actin (Eisenberg et al., 1968).

Steady-State ATPase Experiments. The steady-state ATPase measurements were performed with the use of an automatic pH stat as previously described (Eisenberg & Moos, 1967).

Quenched-Flow Experiments. The quenched-flow experiments were performed in a temperature controlled Durrum D-132 three-syringe quenched-flow apparatus operated in the continuous flow mode as described previously (Chock & Eisenberg, 1979). For measurement of the magnitude of the irreversible binding of ATP, the S-1 was first mixed with about a fivefold molar excess of [γ-^{32}P]ATP with a specific activity of about 5000 cpm/μmol of ATP and then, after a reaction time of 400 ms, quenched with a 500-fold molar excess of nonradioactive ATP from the third syringe. The nonradioactive ATP also contained 2 mM carrier phosphate. The sample was then further incubated for about five half-lives of the steady-state ATPase rate, that is, for about 2–4 min, depending on the reaction conditions prior to quenching with acid. The acid quench and extraction of [^{32}P]P$_i$ were performed as described previously (Chock & Eisenberg, 1979). In studies of the initial P$_i$ burst, the cold ATP quench was replaced with a 2 N HCl solution containing 2 mM carrier phosphate. The extraction of [^{32}P]P$_i$ was performed as described previously (Chock & Eisenberg, 1979) and was based on a modified method of Martin and Doty (Mulhern & Eisenberg, 1976).

Stopped-Flow Experiments. The stopped-flow experiments were performed with the same apparatus as previously described (Rhee & Chock, 1976; Chock et al., 1976). Since the pre-steady-state myosin ATPase reaction is extremely sensitive

Table I: Comparison of the Forward Rate of the Initial P_i Burst with V_{max}

protein	pH	temp (°C)	[KCl] (mM)	max fluorescence rate,[a] $k_5 + k_{-5}$ (s^{-1})	k_5/k_{-5}[b]	k_5 (s^{-1})	V_{max}[d] (s^{-1})	k_5/V_{max}
S-1	7.0	5	0	7.0	1.0[c]	3.5	0.9	3.9
S-1	7.0	15	0	23.2	3.1	17.6	4.3	4.1
S-1	8.0	15	0	38.7	6.7	33.7	5.9	5.7
(A-1)S-1	7.0	15	0	28.0	3.6	21.8	4.0	5.5
S-1	7.0	15	50	41.7	3.6	32.7	5.0	6.5
(A-1)S-1	8.0	15	0	44.9	6.5	39.0	4.7	8.3

[a] Conditions: 10–20 μM S-1; 1.8 mM $MgCl_2$. For experiments at pH 7.0 we used 10 mM imidazole and for experiments at pH 8.0 we used 10 mM Tris. To be certain that the maximum fluorescence rate was achieved, the fluorescence rate was measured at both 1 mM ATP and 2 mM ATP. These two rates were found to be essentially identical, and the value shown is an average of the two rates. [b] Conditions: same as described in footnote *a*. See Materials and Methods and the text for details of how this equilibrium constant was determined. [c] This equilibrium constant was taken from Taylor (1977). [d] Conditions: same as described for Figure 1B except for the determinations at pH 7 where 4 mM imidazole rather than 4 mM Tris was used.

to temperature, the room temperature was adjusted close to the reaction temperature during the experiments. The fluorescence measurements were performed by exciting the sample with incident light of wavelength 300 nm and by measuring the emitted light of wavelength 340 nm at right angles to the incident beam. The wavelength of the incident light was controlled by a Bausch & Lomb monochromator while the wavelength of the emitted light was controlled by a Corian interference filter. In each experiment at least four fluorescence traces were averaged prior to fitting the resultant trace to a first-order rate constant. The data were analyzed in the same manner as before (Chock et al., 1976). Light-scattering experiments were performed using incident light of wavelength 340 nm and measuring the scattered light of wavelength 340 nm at right angles to the incident beam. Experiments involving absorbance of incident light were performed using incident light of 340 nm and measuring the light intensity of the transmitted beam at a wavelength of 340 nm. Absorbance of a sample is then found by taking the log of the ratio of the transmitted light intensity of the buffer to the transmitted light intensity of a particular sample as follows:

$$\text{absorbance} = \log\left[\frac{I(\text{buffer})}{I(\text{sample})}\right]$$

where I(buffer) is the transmitted light intensity of the buffer and I(sample) is that of the sample. Because our apparatus was quite stable, the value of I(buffer) changed only by a few percent during the course of an entire experiment. These changes in I(buffer) were recorded and corrections made to the data in the final analysis.

Results

We began this study by comparing the rate of the initial P_i burst with the maximum actin-activated ATPase rate (V_{max}) under various conditions. V_{max} was determined in the usual manner by plotting 1/ATPase vs. 1/actin (Eisenberg & Moos, 1968). In some cases S-1 containing the alkali 1 light chain [(A-1)S-1] was used since in the double-reciprocal plot of ATPase activity vs. actin (A-1)S-1 shows a lower K_{app} than does the normal mixture of (A-1)S-1 and (A-2)S-1 (Taylor & Weeds, 1977). Thus, V_{max} can be determined more accurately with (A-1)S-1 since, at a given actin concentration, the ATPase activity is closer to V_{max}.

The rate of the initial P_i burst was determined in the absence of actin by making use of the recent finding that most of the fluorescence enhancement induced by ATP is caused by the formation of M**·D·P_i (Johnson & Taylor, 1978; Chock et al., 1979). Of course, at very low ATP concentration the rate of the fluorescence enhancement depends on the rate of ATP binding. But, at high ATP concentration in the absence of actin, the rate of the fluorescence enhancement levels off at its maximum value, and this value is equal to the sum of the forward and reverse rate constants of the initial P_i burst ($k_5 + k_{-5}$ in Scheme II). The forward rate constant (k_5) was then determined by measuring the equilibrium constant between M*·T and M**·D·P_i in the absence of actin. This equilibrium constant was determined by comparing the magnitude of the irreversibly bound ATP (M*·T + M**·D·P_i) with the magnitude of the initial P_i burst (M**·D·P_i) (Chock & Eisenberg, 1979).

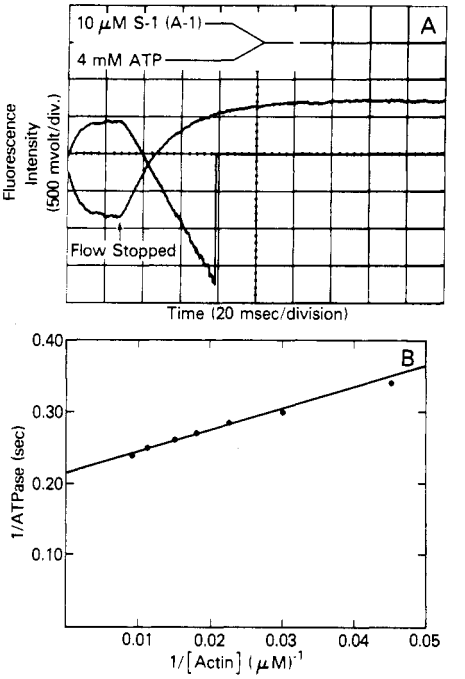

FIGURE 1: Comparison of the maximal rate of the fluorescence enhancement with the V_{max} of the acto–S-1 ATPase cycle. (A) Fluorescence enhancement of (A-1)S-1. Conditions: 5 μM (A-1)S-1; 2 mM ATP; 2.5 mM $MgCl_2$; 10 mM Tris; pH 8.0; 15 °C. The arrow labeled "flow stopped" points to the experimental data. The superimposed linear plot is a computer semilog plot whose slope gives the pseudo-first-order rate constant. (B) Double-reciprocal plot of the acto–S-1 ATPase activity vs. actin concentration; same conditions as described in (A) except here we used 4 mM Tris, 1 μM (A-1)S-1, and F-actin as shown.

Figure 1A shows the time course of the fluorescence enhancement induced by 2 mM ATP at pH 8 with (A-1)S-1; Figure 1B shows a double-reciprocal plot of the (A-1)S-1

ATPase activity vs. actin concentration under the same condition. The rate constant of the fluorescence enhancement is 44 s^{-1}. Since at 2 mM ATP the rate constant of the fluorescence enhancement has leveled off at its maximal value, this rate constant represents the rate constant of the initial P_i burst. The equilibrium constant between M*·T and M**·D·P_i for (A-1)S-1 under this condition was found to be about 6.5 (Table I). Therefore, the forward rate constant from M*·T to M**·D·P_i (k_5) is about 38 s^{-1}. In contrast, V_{max} under this condition is 4.7 s^{-1} (Figure 1B). It therefore appears that with (A-1)S-1 at pH 8, the rate-limiting step in the actomyosin ATPase cycle is not the initial P_i burst.

Table I shows a comparison of V_{max} with the forward rate constant of the initial P_i burst under a number of other conditions. As can be seen, under most conditions the forward rate constant of the initial P_i burst (k_5) is about 5 times faster than V_{max}. This strongly implies that, in general, the initial P_i burst is not the slowest step in the acto–S-1 ATPase cycle. Further evidence that the rate constant for the initial P_i burst does not determine V_{max} comes from the differential effects of pH and ionic strength on V_{max} and the initial P_i burst. Table I shows that an increase in pH from 7.0 to 8.0 or an increase in KCl to 50 mM will almost double k_5 but, as was found previously, will have relatively little effect on V_{max} (Rizzino et al., 1970; Margossian & Lowey, 1973). Therefore, it appears that a step, or a combination of steps, other than the initial P_i burst must play an important role in determining V_{max}.

In the refractory-state model (Scheme II), V_{max} is determined by the rate-limiting transition from the refractory to the nonrefractory state. This transition occurs after the initial P_i burst but before reattachment of the S-1 to actin. Thus, if ATP binding causes complete dissociation of the acto–S-1 complex, this model predicts that almost all of the S-1 should be dissociated from actin even when the ATPase activity is close to V_{max}. In our previous studies at 0 °C, we found that about 20% of the S-1 was bound to actin when the ATPase activity was about 75% of V_{max} (Mulhern & Eisenberg, 1976). The question, therefore, arises whether this binding is due to a small fraction of partially denatured S-1 or whether it is a true feature of the kinetic cycle. It is also important to determine whether the large amount of dissociation observed at 0 °C also occurs at higher temperature. Marston (1978) and Wagner & Weeds (1979) have presented evidence that, at 25 °C, in contrast to 0 °C, this dissociation does not occur as the ATPase approaches V_{max}.

One of the methods we previously used to determine the amount of S-1 complexed with actin during steady-state hydrolysis of ATP at 0 °C was absorbance measured in the spectrophotometer (Fraser et al., 1975). At higher temperatures, however, when the ATPase is close to V_{max}, ATP is hydrolyzed very rapidly. Thus, if enough S-1 is present to give an accurate absorbance measurement, 2–3 mM ATP is hydrolyzed in 1 or 2 min, while if the ATP concentration is increased, the resulting increase in ionic strength causes the ATPase activity to be further away from V_{max}.

To circumvent this problem, we used the stopped-flow apparatus to obtain an accurate measurement of absorbance during the steady-state hydrolysis of ATP at 15 °C. Since a comparison with water could not be made directly in our stopped-flow apparatus, we standardized the instrument by measuring percent transmission rather than absorbance. Each sample measurement was bracketed with voltage measurements on buffer alone to obtain a value for 100% transmission. Zero percent transmission was, of course, the voltage obtained with no light passing through the sample.

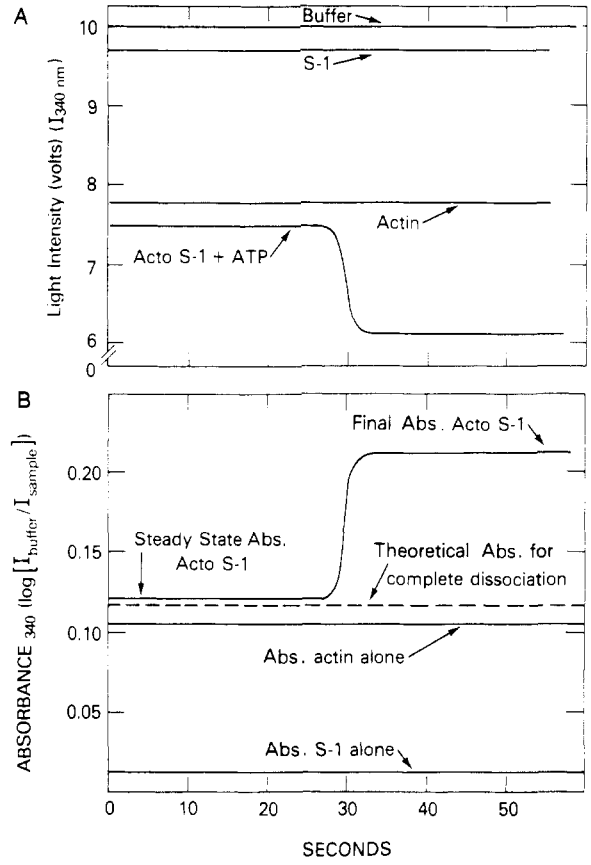

FIGURE 2: Time course of transmitted light intensity and absorbance as measured by the stopped-flow apparatus. (A) Transmitted light intensity (transmittance). Conditions: 58 μM actin; 20 μM S-1; 1 mM ATP; 1.8 mM $MgCl_2$; 50 mM KCl; 10 mM imidazole; pH 7.0; 15 °C. (B) Absorbance as derived from (A) (see the text).

Table II: Effect of the Order of Mixing on the Acto-S-1 Absorbance[a]

syringe 1	syringe 2	steady-state A	final A[b]
actin + S-1	buffer		0.116
actin + S-1	ATP	0.091	0.115
actin + ATP	S-1	0.089	0.112
actin	S-1 + ATP	0.088	0.109

[a] Conditions: 44 μM actin; 10 μM S-1; 1 mM ATP initially; 1.8 mM $MgCl_2$; 10 mM imidazole; pH 7.0; 15 °C. [b] Final absorbance occurs after all of the added ATP is hydrolyzed.

A typical control experiment at 50 mM KCl is shown in Figure 2. Figure 2A shows the actual measured values for percent transmission as a function of time, while Figure 2B shows the calculated absorbance values for the same experiment. As can be seen, while ATP is present, the absorbance of the S-1–actin sample is essentially equal to the sum of the absorbance values for S-1 and actin measured individually. This is what is expected at 50 mM KCl, where, in the presence of ATP, the acto–S-1 complex is almost completely dissociated (Fraser et al., 1975). Of course, after the ATP is completely hydrolyzed, the absorbance of the actin–S-1 sample increases markedly due to the formation of the acto–S-1 complex. We show the actual percent transmission measurements in Figure 2A to demonstrate that the voltage changes which occur during our experiments are quite large. For example, the acto–S-1 complex shows about a 1.5-V change in percent transmission after all of the ATP is hydrolyzed. In contrast, the voltage of the buffer never changed more than 0.1 V during the course of an experiment, and usually no change occurred. Therefore,

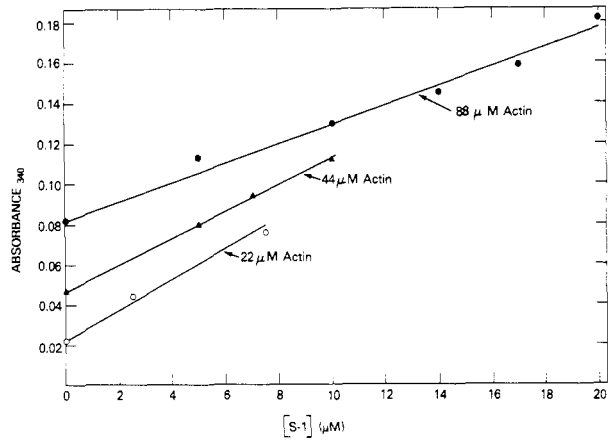

FIGURE 3: Final absorbance of acto–S-1 as a function of S-1 concentration. Final absorbance occurs after all of the added ATP is hydrolyzed. Conditions: 1 mM ATP initially; 1.8 mM $MgCl_2$; 10 mM imidazole; pH 7.0; 15 °C.

the measurements are quite accurate.

We next investigated the acto–S-1 absorbance, in both the presence and the absence of ATP, at very low ionic strength where the ATPase activity approaches V_{max}. We first made certain that the absorbance values obtained in the stopped-flow apparatus at low ionic strength were independent of the method used to prepare the actin–S-1–ATP mixtures. As can be seen in the first three lines of Table II (the last line will be discussed below), the method of mixing the S-1, actin, and ATP has almost no effect on the absorbance values obtained either before or after all of the ATP is hydrolyzed. Whether the ATP is premixed with the actin or mixed with the already formed acto–S-1 complex, the resulting absorbance values are essentially the same. The reproducibility of these absorbance values validates the use of absorbance as a measure of the amount of acto–S-1–ATP complex present. Of course, to use absorbance in this manner requires the assumption that, as was found for acto–S-1–AMP-PNP and acto–S-1 (Greene & Eisenberg, 1978a), the absorbance of acto–S-1–ATP and acto–S-1 is the same. On the basis of this assumption, the absorbance values obtained experimentally can be converted to values for the fraction of S-1 complexed with actin in the presence of ATP.

This conversion was carried out in the following manner. At the low ionic strength where our experiments are performed, all of the S-1 is complexed with actin after the ATP is hydrolyzed. Therefore, by varying the S-1 concentration at a fixed actin concentration, we can obtain a plot of absorbance vs. S-1 bound to actin in the absence of ATP. Several such plots, obtained at different actin concentrations, are shown in Figure 3. There is no theoretical reason why such empirical plots should be linear, and, in fact, they probably bend slightly at high S-1 concentration. Furthermore, the slopes of these plots decrease as the actin concentration increases. Nevertheless, because each plot, itself, is approximately linear, a set of these plots can be obtained in each experiment and then used as empirical standards. In using these plots as standards, we must make a correction for the free S-1 present. This correction was made by assuming that the absorbance of the free S-1 is independent of the amount of actin or acto–S-1 complex present. Although at high actin concentration this assumption may be slightly in error, the contribution of the free S-1 to the total absorbance is so low that the resulting error in the estimate of S-1 bound to actin is less than 10%. Therefore, by using a set of empirical plots such as those shown in Figure 3, we can estimate the amount of S-1 complexed with actin in the presence of ATP.

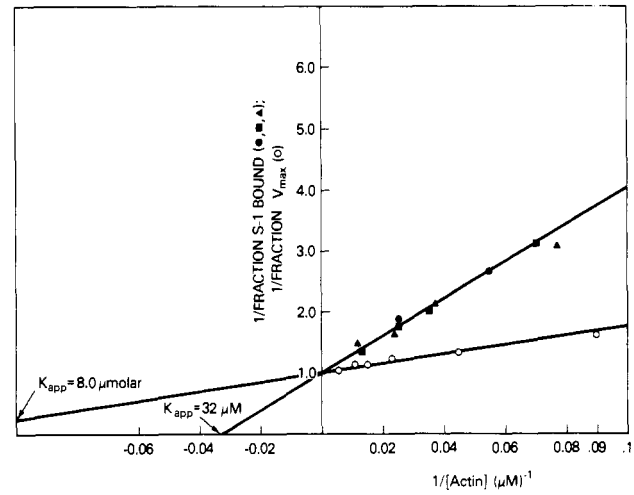

FIGURE 4: Steady-state binding of S-1 to actin in the presence of ATP. Solid symbols: double-reciprocal plot of the fraction of S-1 bound to actin during steady-state ATP hydrolysis vs. actin concentration. Each of the different types of symbols represents a separate experiment. Conditions: 5–20 μM S-1; 1 mM ATP; 1.8 mM $MgCl_2$; 10 mM imidazole; pH 7.0; 15 °C. Open circles: double-reciprocal plot of the acto–S-1 ATPase activity vs. actin concentration. Conditions: same as described for the solid symbols except 1 μM S-1 and 4 mM imidazole were used.

Figure 4 shows a double-reciprocal plot of the fraction of S-1 bound to actin vs. free actin concentration. The experiments shown in this plot were performed at 15 °C in the presence of ATP at very low ionic strength. As can be seen, a significant amount of acto–S-1 complex occurs as the actin concentration is increased. At 90 μM actin, the highest concentration used, 70% of the S-1 is complexed with actin. Furthermore, the double-reciprocal plot is linear, suggesting that the binding shows a simple hyperbolic dependence on actin concentration with 100% of the S-1 binding to actin at infinite actin concentration. These data strongly suggest that the binding we are observing is not due to a small fraction of partially denatured S-1 binding to actin. Furthermore, since this experiment was performed by mixing actin and ATP in one syringe with S-1 in the other, the binding observed cannot be due to incomplete mixing of the acto–S-1 complex with ATP.

For comparison, the open circles in Figure 4 show a double-reciprocal plot of the fraction of maximal ATPase activity (V/V_{max}) vs. free actin concentration. This plot was obtained under the same conditions as the binding data shown in Figure 4. The K_{app} for the binding between S-1 and actin is about 30 μM whereas the K_{app} for the actin-activated ATPase activity is about 8 μM. Therefore, the actin concentration required for half-maximal binding is about 4 times greater than that required for half-maximal ATPase activity. The higher K_{app} for S-1 binding to actin compared to acto–S-1 ATPase activity was observed in all of our experiments under these conditions and is qualitatively similar to our previous observations at 0 °C (Eisenberg & Kielley, 1972; Mulhern & Eisenberg, 1976) which showed that as the ATPase activity approaches V_{max}, a significant fraction of the S-1 is still dissociated from the actin. Marston (1978) also observed, using a kinetic method, that S-1 was partially dissociated from actin at 15 °C, as the ATPase activity approached V_{max}. Nevertheless, our data also show that at high actin concentration, a large amount of the acto–S-1 complex occurs in the presence of ATP. Therefore, the next question which arises is what feature of the kinetic cycle causes this binding.

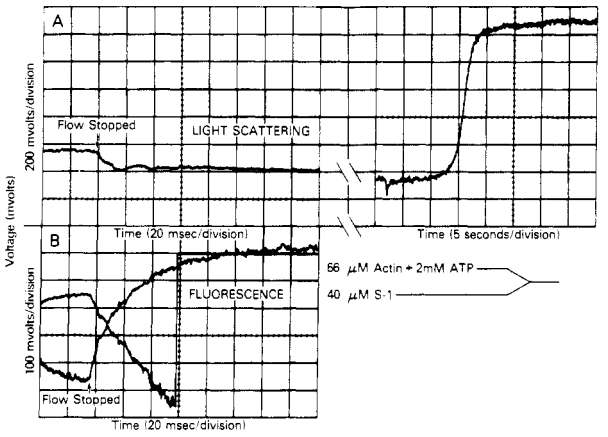

FIGURE 5: Time course of light-scattering and fluorescence changes immediately after the addition of ATP to acto–S-1. Conditions: 33 μM actin; 20 μM S-1; 1.8 mM $MgCl_2$; 1.0 mM ATP; 10 mM imidazole; pH 7.0; 15 °C. At this actin concentration, during the steady-state hydrolysis of ATP, approximately 40% of the S-1 is bound to actin (see the text and Figure 4). (A) Light scattering. (B) Fluorescence enhancement. The arrow labeled "flow stopped" points to the experimental data. The superimposed linear plot is a computer semilog plot whose slope gives the first-order rate constant.

At first, it might appear that the existence of this binding confirms the original postulate of the Lymn–Taylor model (Scheme I) that a slow step in the cycle occurs after reassociation of the S-1 and actin. However, in fact, this need not be the case. Another possibility is that the binding we observe is due to rapid equilibria between actin-free and actin-bound states of S-1 which are shifted toward actin-bound states at high actin concentration. We can distinguish between these two possibilities by determining the time course with which the absorbance reaches its steady-state level. If the binding we observe is due to a rate-limiting step occurring after reassociation of the S-1 and actin, then the steady-state absorbance level will not be reached immediately after the S-1, actin, and ATP are mixed. Rather, immediately after mixing, the absorbance should drop below its steady-state level as the ATP dissociates the acto–S-1 complex. Then, because the S-1 and actin can only reassociate after the initial P_i burst, the absorbance should increase to its steady-state level at about the same rate as the initial P_i burst.

On the other hand, if the binding we observe is due to a rapid equilibrium between M*·T and AM*·T, then the steady-state absorbance should be reached almost instantaneously at 1 mM ATP. This is because the steady-state absorbance will be reached at the rate at which AM*·T and M*·T come to equilibrium, and at 1 mM ATP both the binding of ATP to S-1 or acto–S-1 and the dissociation of the acto–S-1 complex will have rate constants of about 1000 s^{-1} (Lymn & Taylor, 1971; Johnson & Taylor, 1978; Chock et al., 1979). Therefore, M*·T and AM*·T will come to equilibrium with a half-life of about 2 ms, about the dead time of the stopped-flow apparatus.

Figure 5 shows the time courses of the light-scattering and fluorescence changes which occur when 66 μM actin and 2 mM ATP in one syringe are mixed with 40 μM S-1 in the other syringe. At the 33 μM actin concentration used in this experiment, about 45% of the S-1 is complexed with actin during the steady-state hydrolysis of ATP (see Figure 4). Light scattering, rather than absorbance, was measured so that both the change in light scattering and the change in fluorescence could be monitored in the same sample simply by shifting the wavelength of the incident light from 340 to 300 nm. As discussed above, the time course of the fluorescence change represents the time course of the initial P_i burst. As can be seen, the light scattering reaches its steady-state value within 10 ms after the flow stops. Furthermore, the slight decrease in light scattering which was observed during the first 10 ms of the reaction was only a small

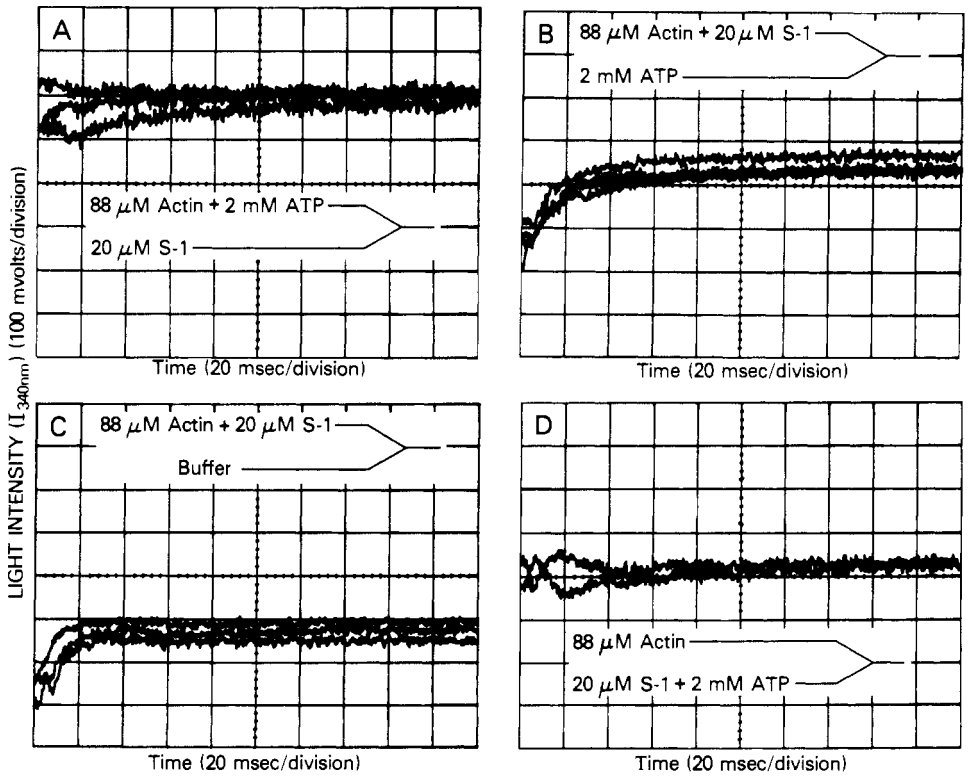

FIGURE 6: Time course of transmitted light intensity immediately after the addition of ATP. Conditions: 44 μM actin; 10 μM S-1; 1 mM ATP; 1.8 mM $MgCl_2$; 10 mM imidazole; pH 7.0; 15 °C. At this actin concentration approximately 50% of the S-1 is bound to actin during the steady-state hydrolysis of ATP (see Figure 4).

fraction of the light-scattering increase which occurred at the end of the reaction when all of the ATP was hydrolyzed. Therefore, the small initial light-scattering decrease is probably a mixing artifact. In any event, the light scattering certainly reaches its steady-state value with a half-life of less than 5 ms. In contrast, as shown by the fluorescence trace, the rate of the initial P_i burst at this actin concentration is about 30 s^{-1}, slightly higher than the rate observed in the absence of actin. Thus, the half-life of the initial P_i burst is about 23 ms. Clearly then, the light scattering reaches its steady-state value before the initial P_i burst occurs.

This result is confirmed by the data presented in Figure 6. In these experiments the time course of the percent transmittance change was determined at an actin concentration of 44 μM where more than 50% of the S-1 is bound to actin during steady-state hydrolysis of the ATP. As can be seen in Figure 6A, when actin and ATP in one syringe were mixed with S-1 in the other syringe, the percent transmittance reached its steady-state value within the dead time of the instrument. Similarly, when acto–S-1 in one syringe was mixed with ATP in the second syringe (Figure 6B), there was only a slight increase in percent transmittance during the first 20 ms of the reaction, and it is very likely that even this small effect is due to a mixing artifact since, as shown in Figure 6C, a similar effect occurs when acto–S-1 is mixed with buffer rather than with ATP. We, therefore, conclude that the binding between S-1 and actin which occurs in the presence of ATP is not due to a rate-limiting step following the reassociation of S-1 and actin as proposed in the original Lymn–Taylor model. Rather, this binding is due to a rapid equilibrium between M*·T and AM*·T, which is shifted toward AM*·T at high actin concentration. The experiments of Sleep & Hutton (1978) showing that actin causes the rapid release of ATP bound to S-1 also provide evidence that M*·T and AM*·T are in rapid equilibrium.

Since a rapid equilibrium occurs between M*·T and AM*·T, it is of great interest to determine whether a similar rapid equilibrium occurs between M**·D·P_i and AM**·D·P_i. It is likely that, during steady-state ATP hydrolysis by acto–S-1, the major unattached S-1 species present is M**·D·P_i because M**·D·P_i occurs just before the rate-limiting step in the acto–S-1 ATPase cycle (Scheme II). The data in Figure 5 show that, in the presence of actin, no change in absorbance occurs during or after the initial P_i burst. The simplest explanation of these data is that M**·D·P_i binds to actin with the same equilibrium constant as that between M*·T and AM*·T.

Another way to determine whether a rapid equilibrium occurs between M**·D·P_i and AM**·D·P_i is to measure the absorbance which occurs when M**·D·P_i is mixed with actin. In our previous experiments where ATP was mixed with the acto–S-1 complex or S-1 was mixed simultaneously with ATP and actin, we were, in effect, determining the equilibrium constant between M*·T and AM*·T since the percent transmittance was measured before hydrolysis of the ATP occurred. However, when ATP is mixed with S-1 alone, the dominant species present in the mixture must be either M**·D·P_i or M‡·D·P_i (Scheme II).

In fact, there are several reasons why, in the absence of actin, it is likely that the major species present in a mixture of S-1 and ATP is M**·D·P_i rather than M‡·D·P_i; i.e., in Scheme II the equilibrium between M**·D·P_i and M‡·D·P_i is shifted toward M**·D·P_i. First, oxygen-exchange data from several laboratories (Bagshaw et al., 1975; Trentham, 1977; Sleep & Boyer, 1978) can be most easily explained by assuming that oxygen exchange is caused by a relatively rapid

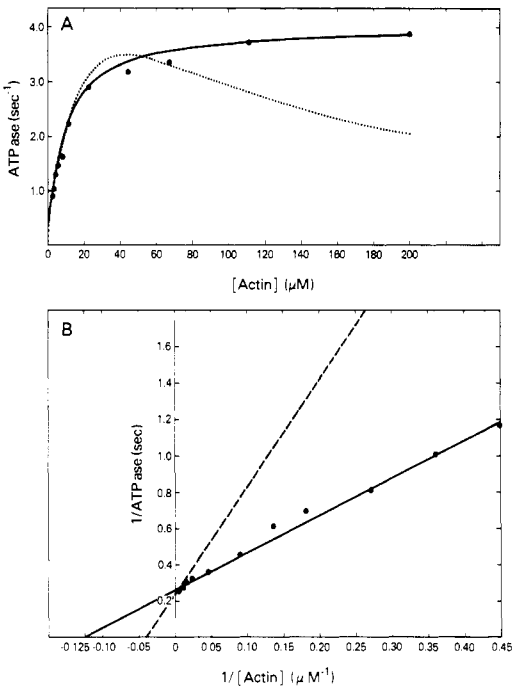

FIGURE 7: Direct and double-reciprocal plot of acto–S-1 ATPase activity vs. actin concentration and theoretical plots for comparison. (A) Direct plots of ATPase activity vs. actin concentration. (B) Double-reciprocal plots of ATPase activity vs. actin concentration. Solid circles: experimental ATPase measurements. Conditions: 1 μM S-1; 1 mM ATP; 1.8 mM $MgCl_2$; 4 mM imidazole; pH 7.0; 15 °C. Dotted line: (A) best fit of the Lymn–Taylor model with k_{10} = 15 s^{-1}. Dashed line: (B) best fit of the upper model in Figure 8 with $k_5 = k_6$ and k_{10} = 8 s^{-1} (see the text and Appendix). Solid lines: plots predicted by the new refractory-state model (see the text and Appendix).

equilibrium between M*·T and M**·D·P_i. If M‡·D·P_i were the major species present in a mixture of S-1 and ATP, a completely different mechanism of ^{18}O exchange would have to be operating. Second, the data in Table I, as well as data from a number of other experiments (Bagshaw & Trentham, 1973; Taylor, 1977; Sleep & Hutton, 1978; Chock & Eisenberg, 1979), show that a considerable amount of M*·T occurs in steady-state mixtures of S-1 and ATP. It is not clear how this could occur if M‡·D·P_i were the dominant species present in a mixture of S-1 and ATP. It therefore appears likely that M**·D·P_i is the major species present during steady-state ATP hydrolysis by S-1 in the absence of actin.

On this basis, we could determine whether a rapid equilibrium occurs between M**·D·P_i and AM**·D·P_i by premixing the S-1 with ATP and then mixing this S-1–ATP solution with actin in the stopped-flow apparatus. Since S-1 hydrolyzes ATP very slowly, a mixture of S-1 and ATP can be introduced into the stopped-flow apparatus and then mixed with actin before a significant fraction of the ATP is hydrolyzed. The results of such an experiment are shown in Figure 6D. As can be seen, just as in the other experiments shown in Figure 6, the transmittance reached its steady-state value within the dead time of the stopped-flow apparatus. Furthermore, as shown in line 4 of Table II, the same steady-state absorbance level was reached when the ATP was premixed with S-1 as when it was premixed with actin. This same result was obtained in numerous experiments at various actin concentrations. We conclude, first, that, just as M*·T is in rapid equilibrium with AM*·T, so too M**·D·P_i is in rapid equilibrium with AM**·D·P_i. Second, we conclude that, at least at very low ionic strength, M*·T and M**·D·P_i bind to actin with the same affinity since mixtures of actin with M*·T or M**·D·P_i show identical absorbance levels. Apparently,

hydrolysis of the ATP on the surface of the S-1 molecule does not significantly affect the binding of the S-1 to actin.

In a kinetic scheme such as the Lymn–Taylor model where hydrolysis of the ATP can occur only after M*·T dissociates from actin, the occurrence of a significant amount of AM*·T should lead to inhibition of the actin-activated ATPase (Lymn, 1974). Since our data suggest that a significant amount of AM*·T occurs at high actin concentration, we measured the actin-activated ATPase activity over a wide range of actin concentration, from 2 to 200 μM. In this way we could determine if there were any changes in the slope of the double-reciprocal plot or any inhibition of the actin-activated ATPase as the actin concentration was increased. As can be seen in Figure 7, no inhibition of the ATPase activity was observed even at 200 μM actin where, on the basis of Figure 4, more than 85% of the S-1 is complexed with actin.

It is possible that slight inhibition of the ATPase activity in this experiment is masked by the fact that the S-1 used is a mixture of (A-1)S-1 and (A-2)S-1. Since (A-1)S-1 and (A-2)S-1 have different values of K_{app} and V_{max} (Taylor & Weeds, 1977), a mixture of the two isoenzymes might yield a double-reciprocal plot which is slightly convex, thus masking the concave plot expected if inhibition of the ATPase occurred. However, we found that a double-reciprocal plot obtained by using purified (A-1)S-1 was also linear up to 90 μM actin. Further detailed ATPase and binding studies with (A-1)S-1 will be necessary. Nevertheless, our data strongly suggest that the actin-activated ATPase activity does not decrease at high actin concentration.

Discussion

In the present study we investigated two questions which are of major importance in understanding the mechanism of the actomyosin ATPase. First, we asked whether the initial P_i burst is the slowest step in the kinetic cycle. Although there have not been any previous measurements actually showing that the initial P_i burst is the slowest step, measurements of the rate of the initial P_i burst at low ionic strength and low temperature have yielded a value of about 7 s^{-1} [Table I and Chock et al. (1976)]. Since the equilibrium constant between M*·T and M**·D·P_i is about 1 at 5 °C (Sleep & Taylor, 1976), this means that the forward rate of the initial P_i burst is about 3 s^{-1}, only 3 times faster than V_{max} measured under similar conditions. Is this threefold difference real or could it be due to experimental error? The results presented in this paper strongly suggest that it is not due to experimental error. We find that, under a number of different conditions, the rate constant of the initial P_i burst is considerably faster than V_{max}, the overall rate constant for ATP hydrolysis (Table I). This conclusion is based on the use of the maximum fluorescence rate as a measure of the rate constant of the initial P_i burst (Johnson & Taylor, 1978; Chock et al., 1979). In addition, however, at 15 °C, pH 7, we have directly measured the rate constant of the initial P_i burst and found it to be at most 20% slower than the rate constant of the fluorescence change (Chock et al., 1979). Therefore, it seems reasonable to conclude that, at a minimum, the forward rate constant of the initial P_i burst is 4 times faster than V_{max}. At higher ionic strength or at pH 8 with (A-1)S-1, the forward rate constant of the initial P_i burst appears to be about 6–8 times faster than V_{max}. Apparently, increases in pH or ionic strength increase the rate constant of the initial P_i burst more than the overall ATPase rate constant, V_{max}, which may explain why previous measurements of the initial P_i burst at 0.1 M KCl, pH 8, were so much faster than V_{max} (Lymn & Taylor, 1971). We therefore conclude that the initial P_i burst is not the slowest step in the ATPase cycle.

The second question which we investigated in the present study is the extent and nature of the binding between S-1 and actin in the presence of ATP. The refractory-state model (Scheme II) in its simplest form predicts that all of the S-1 should be dissociated from actin in the presence of ATP. However, at low temperature Eisenberg and his co-workers (Eisenberg & Kielley, 1972; Mulhern & Eisenberg, 1976) previously found that about 20% of the S-1 and 40% of the HMM were bound to actin when the ATPase activity was about 80% of V_{max}. Furthermore, using a kinetic method, Marston (1978) found that even more binding occurred between S-1 and actin in the presence of ATP at 25 °C than at 5 °C where he confirmed the previous results of Eisenberg & Kielley (1972). Wagner & Weeds (1979) have obtained similar data. The data presented in this paper show that, at 15 °C and at very low ionic strength, binding between S-1 and actin does indeed occur at high actin concentration. At 88 μM actin 70% of the S-1 is bound to actin in the presence of ATP. Furthermore, this S-1 binding shows a simple hyperbolic dependence on actin concentration approaching 100% asymptotically at infinite actin concentration. Thus, the binding between S-1 and actin observed in the presence of ATP is not due to a small fraction of denatured S-1 which cannot be dissociated from actin by ATP. If the actin concentration is high enough, all of the S-1 will bind to actin in the presence of ATP.

What is the nature of this S-1 binding to actin? Lymn & Taylor (1971) found that, at low actin concentration, the binding of ATP rapidly and completely dissociates the acto–S-1 complex. If this rapid and complete dissociation also occurs at high actin concentration, then the presence of a significant amount of S-1 binding to actin during steady-state hydrolysis of ATP must be due to a slow step occurring after reassociation of the S-1 and actin. This is not consistent with the refractory-state model (Scheme II; see the beginning of the text) because the slowest step in this model occurs before reassociation of the S-1 and actin, but it is consistent with the Lymn–Taylor model (Scheme I) because the slowest step in the Lymn–Taylor model occurs after reassociation of the S-1 and actin. However, the Lymn–Taylor model makes the further prediction that the absorbance will drop to a level below its steady-state value immediately after S-1, actin, and ATP are mixed. Then the absorbance will rise to its steady-state value at the relatively slow rate of the initial P_i burst.

In fact, the data presented in this paper clearly show that the absorbance reaches its steady-state level practically within the dead time of the stopped-flow apparatus. Since the absorbance reaches its steady-state value before the initial P_i burst occurs, the binding between S-1 and actin which we observe must be due to incomplete dissociation of the acto–S-1 complex by ATP. That is, a rapid equilibrium develops between AM*·T and M*·T (Scheme I). Since at 1 mM ATP the rate of binding of ATP to S-1 or acto–S-1 will be about 1000 s^{-1} and the subsequent rate of the transition from AM*·T to M*·T is also about 1000 s^{-1} (Lymn & Taylor, 1971; Johnson & Taylor, 1978; Chock et al., 1979), this equilibrium will develop with a half-life of less than 2 ms which is within the dead time of the stopped-flow apparatus. Lymn & Taylor (1971) previously concluded that, at low actin concentration, 1 mM ATP caused extremely rapid and complete dissociation of the acto–S-1 complex. Our data do not conflict with their results since, at low actin concentration, it would be expected that ATP would completely dissociate the acto–S-1 complex. But, at high actin concentration and very low ionic strength, the rapid equilibrium between M*·T and AM*·T is shifted toward AM*·T.

If M**·D·P_i is mixed with actin (by first premixing the S-1 with ATP and then adding this mixture to actin), again the absorbance reaches its steady-state level within the dead time of the stopped-flow apparatus. Furthermore, this absorbance is identical with the absorbance observed when M*·T and AM*·T come to equilibrium. Since equal concentrations of AM*·T and AM**·D·P_i undoubtedly show the same absorbance, these data strongly suggest that the equilibrium constant between AM**·D·P_i and M**·D·P_i is identical with the equilibrium constant between AM*·T and M*·T. This conclusion is supported by our observation that there is no change in absorbance as the initial P_i burst occurs, that is, during the transition from M*·T to M**·D·P_i. Therefore, the simplest interpretation of our data is that both M*·T and M**·D·P_i are in rapid equilibrium with AM*·T and AM**·D·P_i, respectively; in both cases the dissociation constant is about 32 μM under our conditions.

It is of interest that the binding constants of M*·T and M**·D·P_i to actin appear to be nearly identical. Apparently, hydrolysis of ATP on the surface of the S-1 molecule does not affect the affinity of the S-1 for actin. Similarly, the transition from M*·T to M**·D·P_i is accompanied by only a very small decrease in free energy. In contrast, the binding of ATP to S-1 is accompanied by both a marked decrease in free energy (Wolcott & Boyer, 1974; Goody et al., 1977) and a marked decrease in the affinity of S-1 for actin. Apparently, the binding of ATP causes a much greater change in the properties of the S-1 molecule than does the subsequent hydrolysis step.

It may, at first, appear that the binding of M*·T and M**·D·P_i to actin is very weak. However, this binding is actually only about 10-fold weaker than the binding of M-AMP-PNP to actin (Greene & Eisenberg, 1978a; Hofmann & Goody, 1978). ATP weakens the binding of S-1 to actin by a factor of about 10^4, AMP-PNP weakens it by a factor of about 10^3, and ADP weakens it by a factor of about 10^2 (Greene & Eisenberg, 1978b). The value of the dissociation constant of M*·T or M**·D·P_i from actin is 32 μM, and although this appears to be a large dissociation constant, because of the limited range of actin concentration generally employed in in vitro experiments, it in fact represents a reasonably strong binding of S-1 to actin. It is thus quite possible that M*·T and M**·D·P_i are attached to actin filaments in vivo just as M-AMP-PNP is attached to actin filaments (Marston et al., 1976).

How does the value of the dissociation constant of M*·T or M**·D·P_i from actin compare with the value of K_{app}, obtained from the double-reciprocal plot of ATPase activity vs. actin? We have consistently found that, at very low ionic strength and at 15 °C, the dissociation constant is about 4 times larger than K_{app}. This means that, at a given actin concentration, the ATPase activity is considerably closer to V_{max} than the S-1 is to being fully complexed with actin. It seems very unlikely that the fourfold difference which we observe between the K_{app} for the ATPase and the equilibrium constant for binding is due to experimental error. Furthermore, this difference is qualitatively similar to what we have always observed at low temperature; the ATPase activity approaches V_{max} while a considerable fraction of the S-1 remains dissociated from the actin. At the same time, the fact that the equilibrium constant for binding between M*·T or M**·D·P_i and actin is strong enough for binding to occur at high actin concentration explains the small amount of binding we have always observed at low temperature in the presence of ATP.

Despite the binding between M*·T or M**·D·P_i and actin which we observed at high actin concentration, we observe no inhibition of the actin-activated ATPase activity. At 200 μM actin, almost all of the S-1 should be complexed with actin during steady-state hydrolysis of the ATP. Yet, not only have we observed no inhibition of the ATPase, but we have not even been able to detect a decrease in the slope of the double-reciprocal plot at high actin concentration. Thus far, the only report of inhibition of the actin-activated ATPase at high actin concentration has been the data of Marston (1978) at 0 °C where about 10% inhibition was observed at very high actin concentration. Yet at 25 °C, where Marston's kinetic data suggested that considerable binding occurred between the S-1 and actin in the presence of ATP, Marston observed no inhibition of the ATPase. Our results at 15 °C are similar to the data of Marston at 25 °C; no inhibition of the ATPase is observed. Furthermore, preliminary data from our laboratory (see also Figure 5) suggest that the rate of the initial P_i burst measured by determining the maximum fluorescence rate increases rather than decreases as the actin concentration is increased (Stein et al., unpublished experiments).

What kinetic model can we then use to explain our data? Three basic findings must be accounted for by this model. First, the forward rate of the initial P_i burst is about 4 times faster than V_{max}. Second, the dissociation constants of M*·T from AM*·T and of M**·D·P_i from AM**·D·P_i are both 32 μM while K_{app} for the ATPase is about 8 μM. Third, no inhibition of the actin-activated ATPase, and probably no inhibition of the initial P_i burst, occurs at actin concentrations up to 200 μM. Figure 8 shows the two kinetic models we have employed in a computer modeling effort to explain these findings (see Appendix for details of the computer modeling). The upper scheme, with k_6 and k_{-6} approximately equal to zero, is the classic Lymn–Taylor model where hydrolysis of the nucleotide occurs only when the S-1 is dissociated from actin. The heavy solid lines show the dominant pathway in this model. On the basis of the data presented in this paper, we assumed for our computer modeling that, during steady-state hydrolysis of ATP, M*·T is in rapid equilibrium with AM*·T and M**·D·P_i is in rapid equilibrium with AM**·D·P_i, with $K_3 = K_{13} = 32$ μM. We also assumed that $k_5 = 18$ s^{-1} and $k_{-5} = 6$ s^{-1} (Table I). Since ADP release is very rapid and we are working at the saturating ATP concentration, the only variable left in the model is k_{10}. We therefore varied k_{10} in an attempt to match the experimental ATPase data given by the solid circles in Figure 7. The dotted line in Figure 7A shows the best match we could obtain with this model. Here $k_{10} = 15$ s^{-1}. As can be seen, the match is poor. The model predicts that marked inhibition of the actin-activated ATPase should occur at high actin concentration. At 200 μM actin the ATPase should be 60% of what it is at 40 μM actin. In fact, in numerous experiments we have never observed any inhibition of the actin-activated ATPase at high actin concentration. We do not believe that this is just due to experimental error.

The difficulties we encountered in attempting to explain our data with the Lymn–Taylor model were not unexpected since Lymn (1974) showed in a theoretical analysis of the Lymn–Taylor model that, at high actin concentration, inhibition of the ATPase would be expected if the initial P_i burst could only occur when the S-1 was dissociated from actin ($k_6 = 0$). Our computer modeling confirms this analysis. The reason the Lymn–Taylor model was not eliminated previously is that the absorbance data in this paper provide the first direct measure of K_3. Without these data it could not be predicted at what actin concentration ATPase inhibition would first be observed.

Before adding another step to the model, we attempted to

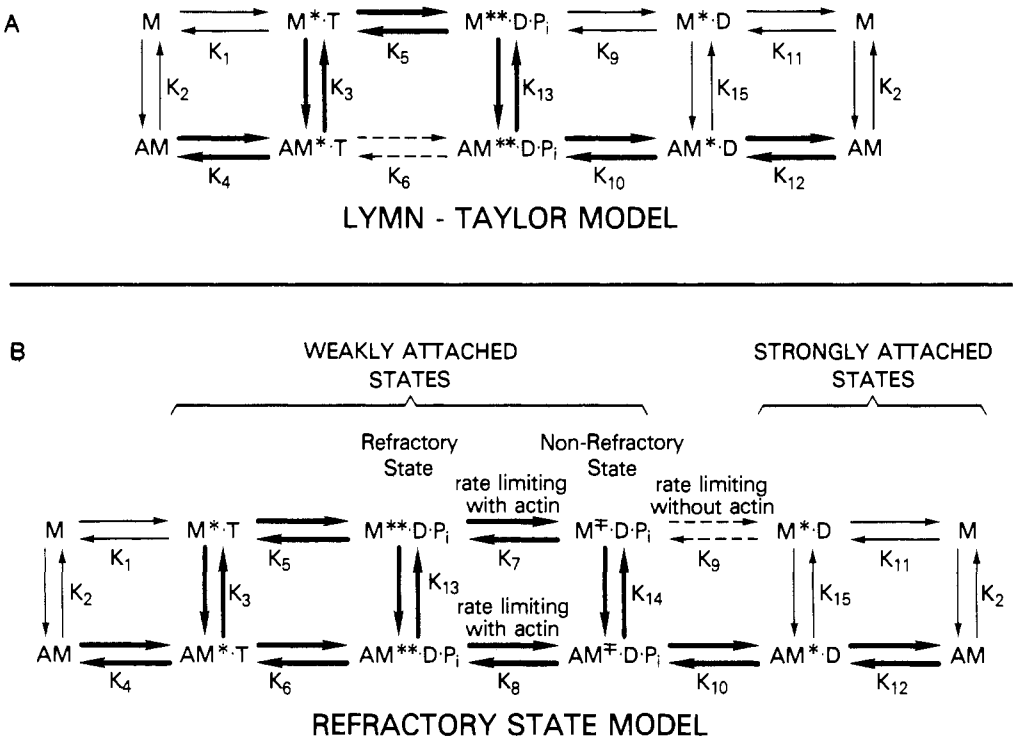

FIGURE 8: Kinetic models of the acto–S-1 ATPase. (A) Lymn–Taylor model: k_6 and k_{-6} are represented by dashed lines because in the original Lymn–Taylor model this step was assumed not to occur. (B) New refractory-state model: k_9 and k_{-9} are represented by dashed lines because $M^{\ddagger}\cdot D\cdot P_i$ may not transform directly to M*·D. It is possible that $M^{\ddagger}\cdot D\cdot P_i$ is a branch of the cycle and M**·D·P_i transforms directly to M*·D in the absence of actin [see Chock et al. (1976)]. In both models, equilibrium constants involving formation of actin complexes are dissociation constants (e.g., K_2 = [A][M]/[AM]). For all other equilibrium constants, products are considered to be to the right of the reactants (e.g., K_1 = [M*·T]/[M][T]).

fit the ATPase data by simply making $k_6 = k_5$, i.e., by allowing the initial P_i burst to occur whether or not the S-1 was bound to actin. The results of this computer modeling are shown by the dashed line in Figure 7B. As expected, this model did not predict inhibition of the ATPase activity at high actin concentration. However, the K_{app} predicted by this computer model was a factor of 3 too high, considerably beyond our experimental error. The reason is that in this computer model K_{app} is approximately equal to K_{13} (see Appendix). White & Taylor (1976) have in the past suggested that K_{app} may equal K_{13}. However, now that we have directly compared K_{app} and K_{13}, we find that K_{app} (8 μM) is significantly less than K_{13} (32 μM). Therefore, to explain our finding that K_{app} is about fourfold smaller than K_{13}, we must introduce another step into the ATPase cycle as shown in the lower scheme (refractory-state model) in Figure 8. With this new scheme, as shown by the solid lines in Figure 7, we can match our data almost perfectly. The reason the refractory-state model works is that the rate-limiting step can occur while the S-1 is dissociated from, as well as attached to, actin. Thus, in the refractory-state model, the value of V_{max} is controlled by k_7 and k_8 while the value of K_{app} is controlled by K_{14}, k_{-7}, k_{-8}, and k_{10} (see Appendix). This means that, even if $K_{14} = K_{13}$, because the value of k_{10} does not significantly affect V_{max}, V_{max} and K_{app} can be independently chosen in this model. Furthermore, because $k_7 = k_8$ and $k_5 = k_6$, no inhibition of the ATPase activity occurs.

In this regard, the results of other recent experiments (Sleep & Hutton, 1978) can also only be explained in terms of a relatively slow step occurring on the dissociated S-1 after the initial P_i burst but before S-1 rebinds to actin. A full explanation of these results also requires the contribution of a nondissociating pathway at high actin concentration as in the refractory-state model in Figure 8. The results of intermediate oxygen-exchange experiments (Sleep & Boyer, 1978) are not consistent with the original refractory-state model (Scheme II), but again, the refractory-state model with a nondissociating pathway in Figure 8 could account for these exchange results. Despite considerable effort, we were unable to fit our linear double-reciprocal plot with a model simpler than the modified refractory-state model in Figure 8 (see Appendix). Therefore, unless there is a major error in our data, this model will probably be required to explain the actomyosin ATPase.

It is important to note that, on the basis of this model, the amount of S-1–actin binding which occurs during steady-state ATP hydrolysis is determined by the values of K_3 and K_{13}, while K_{app} is strongly dependent on the value of K_{14}, k_{-7}, k_{-8}, and k_{10} (see Appendix). Therefore, this model can explain why, at 0 °C, turbidity and ATPase activity do not increase in parallel as the actin concentration is increased. On the other hand, it is true that K_{app}, K_3, and K_{13} are all about the same order of magnitude. This may be because M*·T, M**·D·P_i, and $M^{\ddagger}\cdot D\cdot P_i$, the three myosin nucleotide species where P_i is tightly bound, all may bind to actin with about the same affinity, i.e., $K_3 \simeq K_{13} \simeq K_{14}$. If this were, in fact, the case, then K_{app} would differ from K_3 and K_{13} by a factor which depends mainly on $k_{-8}/(k_{-8} + k_{10})$ (see Appendix). If $k_{-8} > k_{10}$, K_{app} would be approximately equal to K_3 and K_{13}, while if $k_{10} > k_{-8}$, K_{app} would be less than K_3 and K_{13}. Since the values of k_{-8} and k_{10} would certainly vary with temperature and ionic strength, it is quite possible that under certain conditions K_{app} might be about equal to K_3 and K_{13} whereas under other conditions it might be quite different. If this were, in fact, the case, it might explain why, at 25 °C, ATPase activity and turbidity (Marston, 1978; Wagner & Weeds, 1979) seem to increase in parallel whereas at 5 °C they clearly do not.

It should also be noted that this model is still consistent with the pre-steady-state data of Chock et al. (1976). These data showed that, at high actin concentration during a single cycle of ATP hydrolysis, the rate of rebinding of S-1 to actin leveled

off at the same rate as the steady-state ATPase (V_{max}). Our new kinetic model still makes this prediction. However, it also suggests that, as the actin concentration increases, the magnitude of the S-1 dissociated from the actin will decrease. Since in the work of Chock et al. (1976) light scattering rather than absorbance was monitored, this change was not detected.

The kinetic model in Figure 8B is similar to the original refractory-state model (Scheme II) in that a rate-limiting transition (k_8) occurs after the initial P_i burst. It differs from the original refractory-state model in two respects. First, M**·D·P_i can form a complex with actin. Second, both the initial P_i burst and the rate-limiting transition from M**·D·P_i to M‡·D·P_i can occur with the S-1 bound to actin as well as dissociated from actin.

Does it still make sense to describe the rate-limiting transition in this model as a transition from a refractory to a nonrefractory state when, in fact, the refractory state, M**·D·P_i, can undergo this transition when it is either free or bound to actin? We have retained these names for the following reason. Although both the refractory state and the nonrefractory state can bind weakly to actin, the slow transition from the refractory to the nonrefractory state still limits the rate at which S-1 can undergo the subsequent rapid transitions to AM*·D and AM, the states in which S-1 is strongly bound to actin. Thus, rather than a cycle from unattached to attached states occurring, as in the original refractory-state model, a cycle from weakly bound to strongly bound states occurs. Presumably, one of the strongly bound states is the major force-producing state in the muscle (Eisenberg & Hill, 1978). Thus, although the cross bridge in the refractory state may be weakly attached to actin in a rapid equilibrium, it is still blocked from transforming to the major force-producing state, i.e., it is "refractory" in a physiologic sense, until it undergoes a conformational change to the nonrefractory state. This means that, as with the original refractory-state model, the rate-limiting transition from the refractory to the nonrefractory state could still provide the key link between the ATPase rate and the velocity of muscle contraction (Eisenberg et al., 1979). Furthermore, although the original refractory-state model provided an explanation of the velocity of muscle contraction, it also predicted that the number of attached cross bridges would decrease markedly as the velocity increased (Eisenberg et al., 1979), a prediction which is not supported by current X-ray results which suggest, on the contrary, that, as the velocity of muscle contraction increases, the number of attached cross bridges does not significantly decrease (Podolsky et al., 1976). On the other hand, if in vivo the refractory state is weakly attached to actin, the refractory-state model may be compatible with both the current X-ray results and the relationship between the ATPase rate and the velocity.

Three other aspects of this kinetic model are of interest in regard to the mechanism of cross bridge action in vivo. First, this model has no step where the S-1 must detach from actin. If, during the ATPase cycle, the S-1 attached to actin goes from 90 to 45°, it can go back to 90° without first detaching from the actin. This may at first seem impossible physiologically, but, if the weakly attached states are in rapid equilibrium with unattached states and can therefore rapidly detach when they exert negative force, a mandatory detachment step may not be necessary (Eisenberg & Greene, 1980). Second, in the Lymn–Taylor model, it seemed reasonable to assume that AM*·T was a 45° state while AM**·D·P_i was a 90° state since it was postulated that the initial P_i burst could only occur when the S-1 was detached from actin. In our new kinetic model, however, there is no mandatory detachment step, and therefore it is not known which attached states are 90° and which are 45°. Perhaps all of the weakly attached states including AM*·T are 90° states while all of the strongly attached states are 45° states (Eisenberg & Greene, 1980); however, much more work will be necessary to determine if this is indeed the case. Finally, in this kinetic model, since $K_1 \simeq 10^{11}$ M^{-1}, $K_2 \simeq 10^{-8}$ M, and, based on the data in this paper, $K_3 \simeq 10^{-4}$ M, by detailed balance K_4 must be about 10^7 M^{-1}. Therefore, a very large drop in free energy occurs when ATP binds to actomyosin. We believe that this drop in free energy is utilized in some way to produce work in vivo. One of the challenges for future models of muscle contraction will be to suggest ways in which this drop in free energy might be utilized.

Acknowledgments

The expert technical assistance of Louis Dobkin is gratefully acknowledged.

Appendix

The following kinetic model was used as a basis for our steady-state kinetic analysis:

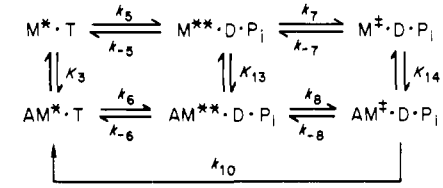

(1)

Here K_3, K_{13}, and K_{14} are dissociation constants; e.g., $K_3 = [A][M^*\cdot T]/[AM^*\cdot T]$.

We assume, on the basis of the data presented in this paper, that M*·T, M**·D·P_i, and M‡·D·P_i are in rapid equilibrium with AM*·T, AM**·D·P_i, and AM‡·D·P_i, respectively. We can then simplify model 1 as follows. We define a rate constant k_5' such that

$$k_5'([M^*\cdot T] + [AM^*\cdot T]) = k_5[M^*\cdot T]$$

Since M*·T and AM*·T are in rapid equilibrium

$$k_5'[M^*\cdot T](1 + [A]/K_3) = k_5[M^*\cdot T]$$

so that $k_5' \equiv k_5/(1 + [A]/K_3) \equiv k_5K_3/([A] + K_3)$. Similarly, we can define a series of other rate constants so that

$$\begin{aligned} k_{-5}' &\equiv \frac{k_{-5}K_{13}}{K_{13} + [A]} & k_{-7}' &\equiv \frac{k_{-7}K_{14}}{K_{14} + [A]} \\ k_6' &\equiv \frac{k_6[A]}{K_3 + [A]} & k_8' &\equiv \frac{k_8[A]}{[A] + K_{13}} \\ k_{-6}' &\equiv \frac{k_{-6}[A]}{K_{13} + [A]} & k_{-8}' &\equiv \frac{k_{-8}[A]}{K_{14} + [A]} \\ k_7' &\equiv \frac{k_7K_{13}}{K_{13} + [A]} & k_{10}' &\equiv \frac{k_{10}[A]}{[A] + K_{14}} \end{aligned} \qquad (2)$$

We can now write a simplified version of model 1

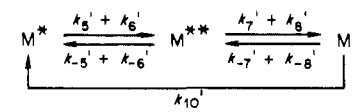

(3)

where $[M^*] = [M^*\cdot T] + [AM^*\cdot T]$, $[M^{**}] = [M^{**}\cdot D\cdot P_i] + [AM^{**}\cdot D\cdot P_i]$, and $[M^‡] = [M^‡\cdot D\cdot P_i] + [AM^‡\cdot D\cdot P_i]$. The steady-state equations for model 3 are

$$[M^*](k_5' + k_6') = [M^{**}](k_{-5}' + k_{-6}') + [M^‡]k_{10}' \qquad (4a)$$

$$[M^{**}](k_{-6}' + k_{-5}' + k_7' + k_8') = [M^*](k_5' + k_6') + [M^\ddagger](k_{-7}' + k_{-8}') \quad (4b)$$

$$[M^\ddagger](k_{-7}' + k_{-8}' + k_{10}') = [M^{**}](k_7' + k_8') \quad (4c)$$

Furthermore, since $[M_{total}] = [M^*] + [M^{**}] + [M^\ddagger]$ and V, the steady-state ATPase rate per micromole of total myosin, is equal to $k_{10}'[M^\ddagger]/[M_{total}]$

$$\frac{1}{V} = \frac{1}{k_{10}'}\left(1 + \frac{[M^*]}{[M^\ddagger]} + \frac{[M^{**}]}{[M^\ddagger]}\right) \quad (5)$$

Substituting eq 4 into eq 7 we have

$$\frac{1}{V} = \frac{1}{k_{10}'}\left[1 + \frac{(k_{10}' + k_{-7}' + k_{-8}')}{(k_7' + k_8')} + \frac{k_{10}'}{(k_5' + k_6')} + \frac{(k_{-5}' + k_{-6}')(k_{10}' + k_{-7}' + k_{-8}')}{(k_5' + k_6')(k_7' + k_8')}\right] \quad (6)$$

Then, substituting the definition in eq 2 into eq 6, we have

$$\frac{1}{V} = \left[\frac{K_{14} + [A]}{k_{10}[A]} + \frac{K_3 + [A]}{k_5K_3 + k_6[A]} + \left[1 + \frac{k_{-5}}{k_5}\frac{(K_3 + [A])}{(K_{13} + [A])}\frac{K_{13}}{K_3}\right]\left[\frac{(K_{13} + [A])(k_{-7}K_{14} + k_{-8}[A] + k_{10}[A])}{k_{10}[A](k_7K_{13} + k_8[A])}\right]\right] \quad (7)$$

This is the general steady-state equation for scheme 1 with the assumption that $M^*{\cdot}T$, $M^{**}{\cdot}D{\cdot}P_i$, and $M^\ddagger{\cdot}D{\cdot}P_i$ are in rapid equilibrium with $AM^*{\cdot}T$, $AM^{**}{\cdot}D{\cdot}P_i$, and $AM^\ddagger{\cdot}D{\cdot}P_i$, respectively.

If we make the further assumption, based on the data presented in this paper, that $K_3 = K_{13}$, eq 7 can be simplified to

$$\frac{1}{V} = \left[\frac{K_{14} + [A]}{k_{10}[A]} + \frac{K_3 + [A]}{k_5K_3 + k_6[A]} + \left(1 + \frac{k_{-5}}{k_5}\right)\left[\frac{[k_{-7}K_{14} + (k_{-8} + k_{10})[A]](K_3 + [A])}{k_{10}[A](k_7K_3 + k_8[A])}\right]\right] \quad (8)$$

This is the general equation for the kinetic model shown in Figure 8B, which, as we will show below, is the simplest kinetic model that can explain our data.

By rearrangement of eq 8, we can put it in the form

$$\frac{1}{V} = \left[\frac{1}{k_{10}} + \frac{1}{k_5} + \left(1 + \frac{k_{-5}}{k_5}\right)\left(\frac{k_{-8} + k_{10}}{k_7k_{10}}\right) + \left(1 + \frac{k_{-5}}{k_5}\right)\left(\frac{K_{14}}{K_3}\right)\left(\frac{k_{-7}}{k_{10}k_7}\right)\left(\frac{k_7 - k_8}{k_7}\right) + \frac{K_{14}}{[A]k_{10}}\left(1 + \left(1 + \frac{k_{-5}}{k_5}\right)\frac{k_{-7}}{k_7}\right) + \left(\frac{[A]}{k_5}\right)\left(\frac{(k_5 - k_6)}{k_5K_3 + k_6[A]}\right) + \left(1 + \frac{k_{-5}}{k_5}\right)\left(\frac{K_{14}}{K_3}\right)\left(\frac{(k_7 - k_8)k_{-7}}{k_7^2}\right)\left(\frac{[A]}{K_{14}k_{-7} + k_{-8}[A]}\right)\right] \quad (9)$$

Note that this rearrangement involves division of several terms by k_7. Therefore, later in this appendix when it is necessary to modify model 1 by assuming $k_7 = 0$, we use eq 8 rather than eq 9 as our basic equation.

Equation 9 has the form

$$\frac{1}{V} = \frac{1}{V_{max}} + \frac{K_{app}}{V_{max}}\frac{1}{[A]} + f([A]) \quad (10)$$

As we will discuss below, the term $f([A])$ goes to 0 when $k_5 = k_6$ and $k_7 = k_8$ in which case eq 9 yields a linear double-reciprocal plot. Note also that the term $f([A])$ goes to 0 as $[A]$ goes to 0 so that eq 9 also yields an approximately linear double-reciprocal plot at low actin concentration. The significance of this point will be discussed below.

We now investigate whether a kinetic model simpler than model 1 can explain our experimental data. We will discuss this equation using eq 9 which, with a simplifying assumption can, of course, be used as the steady-state equation for simpler models. We begin with the Lymn–Taylor model:

$$\begin{array}{ccc} M^*{\cdot}T & \underset{k_{-5}}{\overset{k_5}{\rightleftharpoons}} & M^{**}{\cdot}D{\cdot}P_i \\ {\scriptstyle k_3}\uparrow\downarrow & & \uparrow\downarrow{\scriptstyle k_{13}} \\ AM^*{\cdot}T & \xleftarrow{k_{10}} & AM^{**}{\cdot}D{\cdot}P_i \end{array} \quad (11)$$

The steady-state rate equation for this model is

$$\frac{1}{V} = \frac{1}{k_5} + \left(1 + \frac{k_{-5}}{k_5}\right)\left(\frac{1}{k_{10}}\right) + \left(1 + \frac{k_{-5}}{k_5}\right)\frac{K_3}{k_{10}[A]} + \frac{[A]}{K_3k_5} \quad (12)$$

As shown in Figure 7A, this equation predicts that, at low actin concentration, V, the steady-state ATPase activity, will show a hyperbolic dependence on actin concentration, but at high actin concentration, where the term $[A]/k_5K_3$ becomes significant, the ATPase activity will decrease as the actin concentration increases. The magnitude of this decrease in ATPase activity, over the range of actin where we work, can be easily quantitated in the special cases where the term $f([A])$ is linear with respect to the actin concentration. When this is the case, the actin concentration where the plot of ATPase activity vs. actin reaches a maximum, i.e., the actin concentration where eq 10 reaches a minimum, can be determined by differentiating eq 10 with respect to $[A]^{-1}$ and setting the result equal to 0. As shown in eq 12 for the Lymn–Taylor model, $f([A]) = [A]/K_3k_5$. Therefore, for the Lymn–Taylor model

$$[A]_{minimum} = (k_5K_3K_{app}/V_{max})^{1/2} \quad (13)$$

What is the value of $[A]_{minimum}$ under our conditions? As shown in Figure 7A, the best fit to our experimental data is obtained with the assumption that $k_{10} = 15\ s^{-1}$. Based on the data in this paper showing that $k_5 = 18\ s^{-1}$, $k_{-5} = 6\ s^{-1}$ and $K_3 = 32\ \mu M$. Equation 12 then shows that $K_{app}/V_{max} = 2.8\ \mu M\ s$ and $V_{max} = 7\ s^{-1}$. Therefore, $[A]_{minimum} = 40\ \mu M$. By using eq 10 to determine the steady-state ATPase activity, we can show that, under our conditions, the Lymn–Taylor model predicts a 45% decrease in ATPase activity at 200 μM actin compared to 40 μM actin. Since we have never observed any decrease in ATPase activity, the Lymn–Taylor model cannot explain our data.

A somewhat more complex model is obtained if we add one ($AM^\ddagger{\cdot}D{\cdot}P_i$) or two ($AM^\ddagger{\cdot}D{\cdot}P_i + M^\ddagger{\cdot}D{\cdot}P_i$) more species to the Lymn–Taylor model:

$$\begin{array}{ccccc} M^*{\cdot}T & \underset{k_{-5}}{\overset{k_5}{\rightleftharpoons}} & M^{**}{\cdot}D{\cdot}P_i & & M^\ddagger{\cdot}D{\cdot}P_i \\ {\scriptstyle k_3}\uparrow\downarrow & & {\scriptstyle k_{13}}\uparrow\downarrow & & {\scriptstyle k_{14}}\uparrow\downarrow \\ AM^*{\cdot}T & & AM^{**}{\cdot}D{\cdot}P_i & \underset{k_{-8}}{\overset{k_8}{\rightleftharpoons}} & AM^\ddagger{\cdot}D{\cdot}P_i \\ & \uparrow & & & \uparrow \\ & & {\scriptstyle k_{10}} & & \end{array} \quad (14)$$

The steady-state rate equation for this model is

$$\frac{1}{V} = \frac{1}{k_{10}} + \frac{1}{k_5} + \left(1 + \frac{k_{-5}}{k_5}\right)\left(\frac{k_{-8} + k_{10}}{k_8 k_{10}}\right) + \frac{[A]}{K_3 k_5} + \left[\frac{K_{14}}{k_{10}} + \left(1 + \frac{k_{-5}}{k_5}\right)\left(\frac{k_{-8} + k_{10}}{k_8 k_{10}}\right)K_3\right]\frac{1}{[A]} \quad (15)$$

Although this equation is more complex than eq 12, f([A]) in eq 14 is still equal to $[A]/K_3k_5$. Therefore, $[A]_{minimum}$ will be the same as that found in the Lymn–Taylor model, and this model will predict the same decrease in ATPase activity at high actin concentration as does the Lymn–Taylor model.

Consider next the model

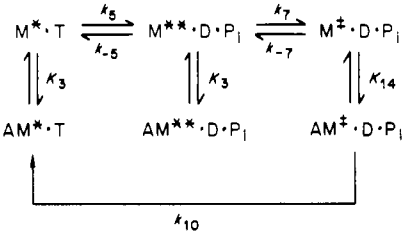

(16)

The steady-state equation for this model is

$$\frac{1}{V} = \frac{1}{k_{10}} + \frac{1}{k_5} + \left(1 + \frac{k_{-5}}{k_5}\right)\left[\left(\frac{1}{k_7}\right) + \frac{k_{-7}K_{14}}{k_7 k_{10} K_3}\right] + \frac{K_{14}}{k_{10}}\left[1 + \left(1 + \frac{k_{-5}}{k_5}\right)\frac{k_{-7}}{k_7}\right]\frac{1}{[A]} + [A]\left[\frac{1}{k_5 K_3} + \left(1 + \frac{k_{-5}}{k_5}\right)\frac{1}{K_3 k_7}\right] \quad (17)$$

Here f([A]) is a considerably larger term than in the preceding models. This is because not only does binding of M*·T to actin decrease the rate of the transition from M*·T to M**·D·P_i as in the preceding models, but, in addition, the binding of M**·D·P_i to actin decreases the rate of the transition from M**·D·P_i to M‡·D·P_i. Therefore, this model predicts an even greater decrease in ATPase activity at high actin concentration than do the preceding models. It also predicts a lower value for $[A]_{minimum}$. Hence, it clearly cannot explain our data.

The following model is the final model which can be drawn where the initial P_i burst does not occur with the S-1 attached to actin:

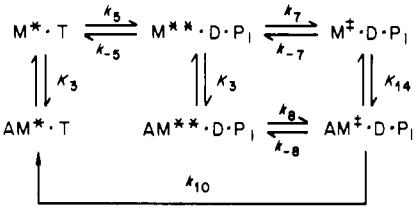

(18)

The steady-state rate equation for this model is

$$\frac{1}{V} = \left[\frac{1}{k_{10}} + \frac{1}{k_5} + \left(1 + \frac{k_{-5}}{k_5}\right)\left(\frac{k_{-8} + k_{10}}{k_7 k_{10}}\right) + \left(1 + \frac{k_{-5}}{k_5}\right)\left(\frac{K_{14}}{K_3}\right)\left(\frac{k_{-7}}{k_{10}k_7}\right)\left(\frac{k_7 - k_8}{k_7}\right) + \frac{K_{14}}{k_{10}[A]}\left[1 + \left(1 + \frac{k_{-5}}{k_5}\right)\frac{k_{-7}}{k_7}\right] + \frac{[A]}{K_3 k_5} + \left(1 + \frac{k_{-5}}{k_5}\right)\left(\frac{K_{14}}{K_3}\right)\left(\frac{k_7 - k_8}{k_7^2}\right)(k_{-7}) \times \left(\frac{[A]}{K_{14}k_{-7} + k_{-8}[A]}\right)\right] \quad (19)$$

This equation has a complex f([A]) term which is the sum of two other terms. The first is the usual term $[A]/k_5K_3$, but the second is a complex term which can be either positive or negative. If $k_7 \geq k_8$, this term will be positive. This model will then show at least as much decrease in ATPase activity at high actin concentration as does the Lymn–Taylor model. On the other hand, if $k_7 \ll k_8$, this model reduces to model 14 which as we have already demonstrated shows a marked decrease in ATPase activity as the actin concentration increases. Since this model cannot explain our data when $k_7 \geq k_8$ or when $k_7 \ll k_8$, it would seem likely that it could not explain our data when $k_7 < k_8$. Direct computer modeling confirmed that this was, indeed, the case. We therefore conclude that no kinetic model with $k_6 = 0$ will fit our experimental data because all such models predict a marked decrease in ATPase activity at high actin concentration.

We now consider a set of models where the initial P_i burst can occur with the S-1 attached to, as well as detached from, actin; i.e., $k_6 \neq 0$. The simplest kinetic model is then

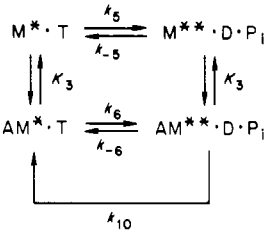

(20)

The steady-state rate equation for this model is

$$\frac{1}{V} = \frac{1}{k_5} + \left(1 + \frac{k_{-5}}{k_5}\right)\frac{1}{k_{10}} + \left(1 + \frac{k_{-5}}{k_5}\right)\left(\frac{K_3}{k_{10}}\right)\frac{1}{[A]} + \left(\frac{[A]}{k_5}\right)\left(\frac{(k_5 - k_6)}{k_5 K_3 + k_6[A]}\right) \quad (21)$$

Consider this model, first, when $k_5 = k_6$. In that case the f([A]) term equals 0, and the double-reciprocal plot of ATPase activity vs. actin predicted by the model is linear.

As can be seen in Figure 7B, under the conditions of our experiment, the slope of the double-reciprocal plot of ATPase activity vs. actin is very close to 2 μM s. Although there may be some ambiguity about the experimental values of K_{app}, K_{app}/V_{max} is known very accurately. Since $k_{-5}/k_5 = 0.33$ and $K_3 = 32$ μM, k_{10} must be 21 s^{-1} for K_{app}/V_{max} to equal 2 μM s (eq 21). However, if $k_{10} = 21$ s^{-1}, V_{max} will equal 8.4 s^{-1}, about twice the experimental value of 4 s^{-1}. Conversely, if k_{10} is assumed to be 7 s^{-1}, V_{max} will be equal to 4 s^{-1}, but K_{app}/V_{max} will be equal to 6 μM s, 3 times the experimental value. Therefore, as shown in Figure 7B, if $k_5 = k_6$ in model 20, this model is not consistent with our experimental data.

If $k_6 > k_5$, then computer modeling shows that the double-reciprocal plot predicted by eq 21 becomes convex so it is even less compatible with our experimental data. However, if k_6 is about one-third of k_5, a small decrease in ATPase activity occurs at high actin concentration, making the double-reciprocal plot somewhat concave. This curvature has a tendency to mask the high value of V_{max} predicted by the model when $K_{app}/V_{max} = 2$ μM s. Therefore, it is possible for model 20 to be consistent with our data if k_6 is less than k_5 but is not zero. However, it is a rather unsatisfactory explanation of our kinetic data: first, because it does not predict a linear double-reciprocal plot, and second, because it requires k_6 to be about one-third k_5 whereas our preliminary fluorescence data suggest that, if anything, k_6 is slightly faster than k_5.

By adding one or two more species to scheme 20, we have the scheme

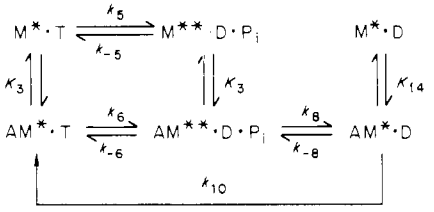

(22)

The steady-state rate equation for this model is

$$\frac{1}{V} = \frac{1}{k_{10}} + \frac{1}{k_5} + \left(1 + \frac{k_{-5}}{k_5}\right)\left(\frac{k_{-8} + k_{10}}{k_8 k_{10}}\right) + \left[\frac{K_{14}}{k_{10}} + \left(1 + \frac{k_{-5}}{k_5}\right)\left(\frac{k_{-8} + k_{10}}{k_8 k_{10}}\right)K_3\right]\frac{1}{[A]} + \left(\frac{[A]}{k_5}\right)\left(\frac{(k_5 - k_6)}{k_5 K_3 + k_6[A]}\right) \quad (23)$$

This model might explain our steady-state kinetic data if $k_{10} \simeq k_8$ and $K_{14} < K_3$. At the same time, however, if k_{10} is made this slow and $K_{14} < K_{13}$, this model becomes inconsistent with our pre-steady-state kinetic data. The reason is that state $AM^{\ddagger}\cdot D\cdot P_i$ becomes a significant species and therefore this model predicts that, after mixing S-1, ATP, and actin, the absorbance will first drop below its steady-state level and then increase to its steady-state level as state $AM^{\ddagger}\cdot D\cdot P_i$ is formed. Since we never observe such a change in absorbance, this model, with k_{10} assumed to be slow, is not consistent with our pre-steady-state kinetic data. On the other hand, if $k_{10} \gg k_8$, this model becomes identical to scheme 20, discussed above.

The final model of this type which can occur is

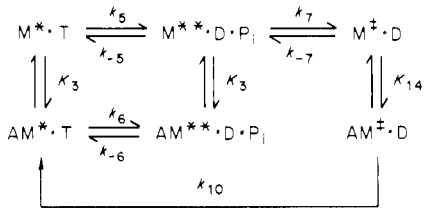

(24)

The steady-state rate equation for this model is

$$\frac{1}{V} = \frac{1}{k_{10}} + \frac{1}{k_5} + \left(1 + \frac{k_{-5}}{k_5}\right)\left(\frac{1}{k_7} + \frac{k_{-7}K_{14}}{k_{10}k_7K_3}\right) + \frac{K_{14}}{k_{10}}\left[1 + \left(1 + \frac{k_{-5}}{k_5}\right)\frac{k_{-7}}{k_7}\right]\frac{1}{[A]} + \frac{[A]}{K_3k_7}\left(1 + \frac{k_{-5}}{k_5}\right) + \frac{[A]}{k_5}\left(\frac{(k_5 - k_6)}{k_5K_3 + k_6[A]}\right) \quad (25)$$

Although f([A]) in this model is a rather complex function of [A], computer modeling shows that the inhibition caused by k_8 being zero will overcome any activation caused by $k_6 > k_5$. Therefore, like many of the preceding models, this model predicts a considerable decrease in ATPase activity at high actin concentration, a decrease which we have never observed experimentally.

In this appendix we have examined the various kinetic models which might explain our data. Except for the original model shown in Figure 8B, all but one of these models are unsatisfactory, predicting either a marked decrease in ATPase activity at high actin concentration or erroneous values for V_{max} or K_{app}. Only model 20 comes close to explaining our data, and it does so in a rather artificial manner by having an inhibitory term mask a high value of V_{max}. Furthermore, this model requires k_6 to be considerably less than k_5. Preliminary experimental results suggest that this is not the case, but further experiments will be required to completely rule out this model.

The kinetic model which best explains our data is the model shown in Figure 8B, i.e., model 1. Equation 9 gives the steady-state rate equation for this model. If $k_5 = k_6$ and $k_7 = k_8$, this model is described by the steady-state rate equation

$$\frac{1}{V} = \frac{1}{k_{10}} + \frac{1}{k_5} + \left(1 + \frac{k_{-5}}{k_5}\right)\left(\frac{k_{-8} + k_{10}}{k_8 k_{10}}\right) + \frac{1}{[A]}\frac{K_{14}}{k_{10}}\left[1 + \left(1 + \frac{k_{-5}}{k_5}\right)\frac{k_{-7}}{k_7}\right] \quad (26)$$

This equation predicts a linear double-reciprocal plot. Furthermore, with the assumption that $K_3 = K_{13} = K_{14} = 32\ \mu M$, $k_5 = k_6 = 18\ s^{-1}$, $k_{-5} = k_{-6} = 6\ s^{-1}$, $k_7 = k_8 = 10\ s^{-1}$ and by choosing k_{10} and k_{-7} so that $(k_{10} - 16)/k_{-7} = 2.1$, this model predicts the solid line shown in Figure 7B ($V_{max} = 4\ s^{-1}$; $K_{app} = 8\ \mu M$) and is therefore consistent with our experimental data. Note that our experimental data do not uniquely determine k_{-7} and k_{10}. However, k_{-7} and k_{10} must be consistent with the above expression for eq 26 to be consistent with our experimental data.

If, as discussed under Results, $k_{-7} > k_7$ and, in addition, we make the simplifying approximation that k_5 and k_{10} do not contribute to V_{max}, eq 26 predicts that $V_{max} = k_8k_{10}/(k_{-8} + k_{10})$ and $K_{app} = K_{14}k_{-7}/(k_{-8} + k_{10}) = K_3k_{-8}/(k_{-8} + k_{10})$. This latter equivalence occurs because we assumed that $k_7 = k_8$. Therefore, by detailed balance $K_{14}k_{-7} = K_3k_{-8}$.

References

Bagshaw, C. R., & Trentham, D. R. (1973) *Biochem. J. 133*, 323–328.

Bagshaw, C. R., Eccleston, J. F., Eckstein, F., Goody, R. S., Gutfreund, H., & Trentham, D. R. (1974) *Biochem. J. 141*, 351–364.

Bagshaw, C. R., Trentham, D. R., Wolcott, R. G., & Boyer, P. D. (1975) *Proc. Natl. Acad. Sci. U.S.A. 72*, 2592–2596.

Chock, S. P., & Eisenberg, E. (1979) *J. Biol. Chem. 254*, 3229–3235.

Chock, S. P., Chock, P. B., & Eisenberg, E. (1976) *Biochemistry 15*, 3244–3253.

Chock, S. P., Chock, P. B., & Eisenberg, E. (1979) *J. Biol. Chem. 254*, 3236–3243.

Eisenberg, E., & Moos, C. (1967) *J. Biol. Chem. 242*, 2945–2951.

Eisenberg, E., & Moos, C. (1968) *Biochemistry 7*, 1486–1489.

Eisenberg, E., & Moos, C. (1970) *J. Biol. Chem. 245*, 2451–2456.

Eisenberg, E., & Kielley, W. W. (1972) *Cold Spring Harbor Symp. Quant. Biol. 37*, 145–152.

Eisenberg, E., & Kielley, W. W. (1974) *J. Biol. Chem. 249*, 4742–4748.

Eisenberg, E., & Hill, T. L. (1978) *Prog. Biophys. Mol. Biol. 33*, 55–82.

Eisenberg, E., & Greene, L. (1980) *Annu. Rev. Physiol.* (in press).

Eisenberg, E., Zobel, C. R., & Moos, C. (1968) *Biochemistry 7*, 3186–3194.

Eisenberg, E., Hill, T. L., & Chen, Y. (1979) *Biophys. J.* (in press).

Fraser, A. B., Eisenberg, E., Kielley, W. W., & Carlson, F. D. (1975) *Biochemistry 14*, 2207–2214.

Goody, R. S., Hofmann, W., & Mannherz, H. (1977) *Eur. J. Biochem. 78*, 317–324.
Greene, L. E., & Eisenberg, E. (1978a) *Proc. Natl. Acad. Sci. U.S.A. 75*, 54–58.
Greene, L. E., & Eisenberg, E. (1978b) *Biophys. J. 21*, 17a.
Hofmann, W., & Goody, R. S. (1978) *FEBS Lett. 89*, 169–172.
Huxley, A. F. (1974) *J. Physiol. (London) 243*, 1–43.
Huxley, H. E. (1969) *Science 164*, 1356–1366.
Johnson, K. A., & Taylor, E. W. (1978) *Biochemistry 17*, 3432–3442.
Kielley, W. W., & Harrington, W. F. (1960) *Biochim. Biophys. Acta 41*, 401–421.
Lymn, R. W. (1974) *J. Theor. Biol. 43*, 313–328.
Lymn, R. W., & Taylor, E. W. (1971) *Biochemistry 10*, 4617–4624.
Margossian, S. S., & Lowey, S. (1973) *J. Mol. Biol. 74*, 313–330.
Marston, S. B. (1978) *FEBS Lett. 92*, 147–151.
Marston, S. B., Rodger, C. D., & Tregear, R. T. (1976) *J. Mol. Biol. 104*, 263–276.
Mulhern, S., & Eisenberg, E. (1976) *Biochemistry 15*, 5702–5707.
Podolsky, R. J., St. Onge, R., Yu, L., & Lymn, R. W. (1976) *Proc. Natl. Acad. Sci. U.S.A. 73*, 813–817.
Rhee, S. G., & Chock, P. B. (1976) *Biochemistry 15*, 1755–1760.
Rizzino, A. A., Barouch, W. W., Eisenberg, E., & Moos, C. (1970) *Biochemistry 9*, 2402–2408.
Sleep, J. A., & Taylor, E. W. (1976) *Biochemistry 15*, 5813–5817.
Sleep, J. A., & Boyer, P. D. (1978) *Biochemistry 17*, 5417–5422.
Sleep, J. A., & Hutton, R. L. (1978) *Biochemistry 17*, 5423–5430.
Spudich, J. A., & Watt, S. (1971) *J. Biol. Chem. 246*, 4866–4871.
Stein, L., Schwarz, R. P., & Eisenberg, E. (1979) *Biophys. J. 25*, 20a.
Taylor, E. W. (1977) *Biochemistry 16*, 732–740.
Taylor, R. S., & Weeds, A. G. (1977) *FEBS Lett. 75*, 55–60.
Trentham, D. R. (1977) *Biochem. Soc. Trans. 5*, 5–22.
Wagner, P. D., & Weeds, A. G. (1979) *Biochemistry 18*, 2260–2266.
Weeds, A. G., & Taylor, R. S. (1975) *Nature (London) 257*, 54–56.
White, H. D., & Taylor, E. W. (1976) *Biochemistry 15*, 5818–5826.
Wolcott, R. G., & Boyer, P. D. (1974) *Biochem. Biophys. Res. Commun. 57*, 709–716.

Purification of Opsonically Active Human and Rat Cold-Insoluble Globulin (Plasma Fibronectin)†

Janos Molnar,* Frank B. Gelder, Ming Zong Lai, Gerald E. Siefring, Jr., R. Bruce Credo, and Laszlo Lorand

ABSTRACT: Two different affinity chromatographic procedures were developed for the purification of opsonin from plasma or serum, utilizing either heparin or specific antibody containing columns. Activities were measured in liver tissues by the uptake of ^{125}I-labeled latex particles to which gelatin was covalently coupled. Regardless of whether the proteins were derived from human or rat blood, opsonic potencies of the purified products were very similar to that of human cold-insoluble globulin (CIG or fibronectin) obtained as a byproduct in the course of factor XIII fractionation by the method of Lorand & Gotoh [Lorand, L., & Gotoh, T. (1970) *Methods Enzymol. 19*, 770–782]. As judged by electrophoretic and immunological criteria, all procedures yielded materials of similar purity. Furthermore, human and rat opsonins cross-react immunologically. The hepatic system appears to be quite specific for gelatinized particles, because no uptake could be accomplished when fibrinogen, fibrin, or serum albumin was coupled to latex. In competition assays, only gelatin or collagen added in solution caused an inhibition of the uptake of gelatinized particles, while fibrinogen or serum albumin had no effect. In addition to the opsonic protein, some constituent of commercial heparin, other than that responsible for the anticoagulant activity of this mucopolysaccharide mixture, is required for promoting the hepatic uptake of gelatinized latex particles. Further support for the identity of opsonin with CIG, first suggested by Blumenstock and co-workers [Blumenstock, F. A., Saba, T. M., Weber, P., & Loffin, R. (1978) *J. Biol. Chem. 253*, 4387–4291], was obtained by showing that the opsonic activity of a solution could be reduced considerably by the process of specific cross-linking by factor $XIII_a$ in the presence of fibrin.

Phagocytosis is the specialized function of certain cells in higher organisms involved in host defense with the purpose of ingesting and digesting harmful particles such as bacteria, antigen–antibody complexes, tissue debris, and colloidal pollutants. It has many similarities to the transport of low molecular weight nutrients (salts, amino acids, and sugars) and, in addition, it depends on humoral recognition factors (opsonizing factors) which give the process selectivity and efficiency (DiLuzio et al., 1971). So far at least two opsonizing systems have been recognized. One is related to the removal of antibody-coated antigenic particles, often involving the participation of a complement (Gigli & Nelson, 1968; Morelli & Rosenberg, 1971; Moreau & Skarnes, 1975). The other system, relating to the subject matter of our work, seems to be specific for the phagocytosis of collagen- or gelatin-coated

† From the Department of Biological Chemistry, University of Illinois, Chicago, Illinois 60612 (J.M. and M.Z.L.), Louisiana State University, Medical Center, Shreveport, Louisiana 71130 (F.B.G.), and the Department of Biochemistry and Molecular Biology, Northwestern University, Evanston, Illinois 60201 (G.E.S., R.B.C., and L.L.). *Received March 13, 1979.* This work was supported at the University of Illinois by a grant from the National Institutes of Health (9 R01 CA 2504) and one from the University of Illinois Campus Research Board, at Louisiana State University by Immunodiagnostic Products, Ltd., Chicago, IL 60660, and at Northwestern University by U.S. Public Health Service Career Award 5 K06 HL 03512 and by a grant from the National Heart, Lung and Blood Institute (HL 02212).

0006-2960/79/0418-3909$01.00/0